

# Two dimensional ferroelectric domain patterns in $\text{Yb}^{3+}$ optically active $\text{LiNbO}_3$ fabricated by direct electron beam writing

L. Mateos, L. E. Bausá, and M. O. Ramírez

*Dpto. Física de Materiales and Instituto Nicolás Cabrera, Universidad Autónoma de Madrid, 28049 Madrid, Spain*

(Received 21 December 2012; accepted 18 January 2013; published online 1 February 2013)

We report on highly controllable ferroelectric domain inversion in  $\text{Yb}^{3+}$  doped  $\text{LiNbO}_3$  laser crystal. The ferroelectric domain patterns are fabricated by direct electron beam writing without any previous masking process. Square lattices of inverted domains with diameters and distance between domains as low as  $1\text{ }\mu\text{m}$  are demonstrated. The lateral growth of the inverted domains is analyzed as a function of the applied charge and the threshold values for domains in the  $1\text{--}10\text{ }\mu\text{m}$  length scale are determined. Spatially resolved low temperature fluorescence spectroscopy and non-collinear second harmonic generation experiments are also employed to evaluate the optical properties of the system. © 2013 American Institute of Physics. [<http://dx.doi.org/10.1063/1.4790149>]

A next generation of photonic and optoelectronic devices is now being developed by using ferroelectric crystals as multifunctional optically active substrates. The interest of these systems not only arises from their attractive electro-optic, piezoelectric, or pyroelectric properties but also from the possibility of shaping ferroelectric domains with opposite polarity at the micro and sub-micrometer scale, thus, providing unique performances. In fact, ferroelectric domain engineering is at the heart of a large variety of optical devices currently used in several scientific and technologically relevant fronts owing to the key role of frequency conversion processes on the generation and later control of light distribution.<sup>1–3</sup>

A step further on ferroelectric based light control devices can be obtained by exploiting the intrinsic emission properties of optically active ferroelectric materials. In the last years, the use of ferroelectric crystals as host matrices for laser ions has emerged as an alternative to develop multifunctional solid state lasers capable to generate infrared laser action and simultaneously visible radiation by self-frequency conversion processes.<sup>4</sup> Further, by using photochemical methods, metallic silver nanoparticles were deposited on an  $\text{Nd}^{3+}$  doped periodically poled  $\text{LiNbO}_3$  crystal, to produce periodic intensification of both the nonlinear response and the spontaneous emission of  $\text{Nd}^{3+}$  ions.<sup>5</sup> Nevertheless, despite the potential of these systems, the control of ferroelectric domain engineering in optically active ferroelectric crystals still remains challenging, particularly when the ferroelectric patterning is extended to two dimensional (2D) geometries.

Here, we report on the fabrication and optical characterization of highly controllable 2D ferroelectric domain patterns in  $\text{Yb}^{3+}$  doped bulk  $\text{LiNbO}_3$  laser crystal by using direct electron beam writing (DEBW). This technique has already been used to tailor stable ferroelectric structures in  $\text{LiNbO}_3$ .<sup>6–8</sup> However, several issues concerning scalability, minimum size, and distances between inverted domains or their growth evolution with the applied charge still require further investigation. Here, the lateral growth of the inverted domains in the  $x$ - $y$  plane is analyzed in terms of the so called ferroelectric domain breakdown phenomenon<sup>9</sup> and the

charge threshold values for inverted domains in the  $1\text{--}10\text{ }\mu\text{m}$  length scale are determined. On this basis, large areas ( $0.5 \times 0.5\text{ mm}^2$ ) of fully dense 2D regular alternate ferroelectric domains with diameters as low as  $1\text{ }\mu\text{m}$  in  $500\text{ }\mu\text{m}$ -thick plates from congruent  $\text{Yb}^{3+}:\text{LiNbO}_3$  bulk crystal are demonstrated. Low temperature (LT) fluorescence spectroscopy and non-collinear second harmonic generation (SHG) experiments were also employed to confirm that the applied charge densities do not alter either the spectroscopic properties of  $\text{Yb}^{3+}$  ion or the nonlinear response of the system.

The irradiation process was performed by directly focusing the e-beam on the  $-z$  face of the crystal by means of a Philips XL30 Schottky field emission gun electron microscope driven by an ELPHY RAITH software. Prior to irradiation, a  $100\text{ nm}$  film of Al was deposited on the  $+z$  face, which acts as a ground electrode. The applied charge density was varied from  $600\text{ }\mu\text{C}/\text{cm}^2$  up to  $3000\text{ }\mu\text{C}/\text{cm}^2$ . The acceleration voltage and the beam current were set at  $15\text{ kV}$  and  $0.3\text{ nA}$ , respectively. Selective chemical etching in a 2:1 solution of  $\text{HNO}_3:\text{HF}$  was employed to reveal the domain structures. The  $\text{Yb}^{3+}$  concentration in the crystal was  $0.5\text{ wt. \%}$ .

Figures 1(a) and 1(b) show the scanning electron microscope (SEM) images of  $\text{Yb}^{3+}:\text{LiNbO}_3$  on which two sets of square lattices of hexagonal shaped inverted ferroelectric domains for different values of the electronic charge density are revealed. The diameters of the irradiated single motives were  $7\text{ }\mu\text{m}$  (Fig. 1(a)) and  $1\text{ }\mu\text{m}$  (Fig. 1(b)), respectively. Two effects are observed. On one hand the smaller the irradiated motif, the higher the electronic charge density required to reverse the spontaneous polarization. For instance, the irradiation of motives with a diameter of  $7\text{ }\mu\text{m}$  with an electronic charge density of  $1000\text{ }\mu\text{C}/\text{cm}^2$  produces ferroelectric inversion and arrays of inverted hexagonal ferroelectric domains as observed (Fig. 1(a)). However, when the irradiated motives are limited to  $1\text{ }\mu\text{m}$ , no ferroelectric inversion is observed for the same charge density (Fig. 1(b)). Figure 1(c) shows the minimum electronic charge density required to produce effective polarization reversal as a function of the diameter of the irradiated motives in the range  $1\text{--}10\text{ }\mu\text{m}$ . Two different samples thickness,  $500\text{ }\mu\text{m}$  and  $400\text{ }\mu\text{m}$ , were

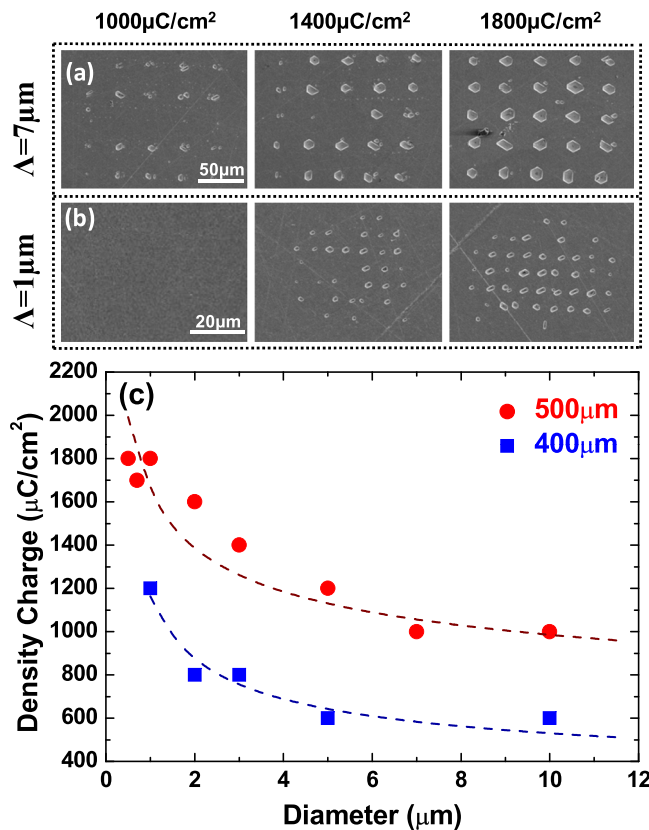


FIG. 1. SEM images of hexagonal shaped inverted domains as a function of the electronic charge density in  $\text{Yb}^{3+}:\text{LiNbO}_3$ . The diameters of the irradiated motives are: (a)  $\Lambda = 7 \mu\text{m}$  and (b)  $\Lambda = 1 \mu\text{m}$ . (c) Threshold values as a function of the diameter of the irradiated motives. Lines are a guide for the eye.

studied. As expected, the minimum charge density required to reverse the spontaneous polarization increases with the sample thickness. In both samples, a clear reduction in the charge density threshold is observed when increasing the size of the irradiated motif. We will go back to this point next.

On the other hand any further increase of the electronic charge density above the threshold value allows domain reversal to occur spontaneously leading to a lateral expansion of the inverted motives. Note that for an electronic charge density of  $1800 \mu\text{C}/\text{cm}^2$ , the obtained domain diameter after irradiating a  $7 \mu\text{m}$  motif is, in average, of around  $15 \mu\text{m}$ .

Figure 2 describes the behavior of the lateral domain growth. There, the final diameter is depicted as a function of the applied charge. As seen, the domain size follows a power law with the applied charge, which can be fitted to an exponent of  $2/3$  when the diameter of the inverted domains is  $< 10 \mu\text{m}$ . In this case, for  $500 \mu\text{m}$ -thick crystals, the radius of the inverted domains,  $r$ , is about 2 orders of magnitude smaller than their length,  $l$ . Therefore, the obtained lateral domain size dependence on the applied charge agrees well with the equilibrium domain dimensions previously predicted for string-like shape domains ( $r \ll l$ ),<sup>9</sup> where the switching occurs upon the high inhomogeneous electric field induced by a point source as the one provided by the e-beam and the inverted motif grows to its equilibrium shape, which is determined by the free energy minimum condition.<sup>9</sup> Such a growth process accounts for both the observed threshold

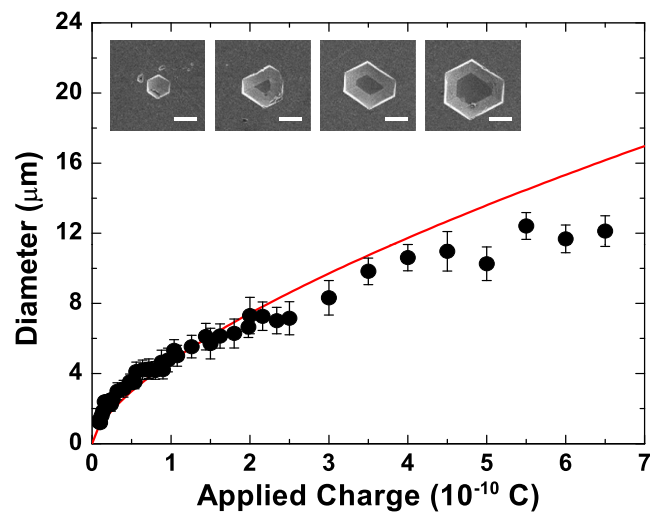


FIG. 2. Lateral growth of the inverted ferroelectric domains as a function of the applied charge. The inset shows the growth evolution of a single irradiated motif upon different applied charges.

values and the lateral domain expansion as a function of the applied charge, and allows determining the experimental conditions for tailoring ferroelectric structures with short sizes and periods as desired for advanced photonic materials. For larger domain sizes, a deviation from the  $2/3$  exponent is observed, probably because the string-like shape approximation is not longer valid. Other considerations such as bulk screening or a large concentration of pinning centers can also be invoked.<sup>10</sup>

Several periodical patterns of ferroelectric domains with different sizes and geometries were then irradiated on the basis of the above analysis. The results are shown in Figure 3. The panels were chosen to illustrate not only the feasibility of the technique to produce large area of regular alternate ferroelectric domain in 2D geometries but also the possibility to control the filling factor parameter in ferroelectric structures with inverted diameters as low as  $1 \mu\text{m}$ .

Spatially resolved LT fluorescence spectroscopy and non-collinear SHG experiments were used to analyze the effect of the electronic irradiation on the optical properties of  $\text{Yb}^{3+}$  doped  $\text{LiNbO}_3$  crystals. It has been established that trivalent rare earth (RE) ions substitute for  $\text{Li}^+$  in  $\text{LiNbO}_3$ . These ions are off-centered from the regular Li position due to the presence of different charge compensation mechanisms, and so they may exhibit a multi-center distribution due to their slightly different local environment.<sup>11</sup> Due to the strong re-arrangement of the crystal lattice during the polarization reversal, the spectral features of non-equivalent RE centers can be altered, as previously shown.<sup>12,13</sup> In  $\text{LiNbO}_3$ ,  $\text{Yb}^{3+}$  ion exhibits a single major emitting center.<sup>14</sup> To investigate about the possible perturbations in the local structure of  $\text{Yb}^{3+}$  center in  $\text{LiNbO}_3$  after the e-beam irradiation, the spectroscopic properties of this ion have been analyzed in the original and inverted regions. Figure 4(a) shows the LT (10 K) emission spectra obtained under excitation at the  $F_{7/2}(0) \rightarrow F_{5/2}(2')$  of  $\text{Yb}^{3+}$  ions (930 nm). They consist of four main optical bands located at around 980 nm, 1005 nm, 1030 nm, and 1060 nm, which can be associated with the transitions from the lowest Stark energy level of the excited

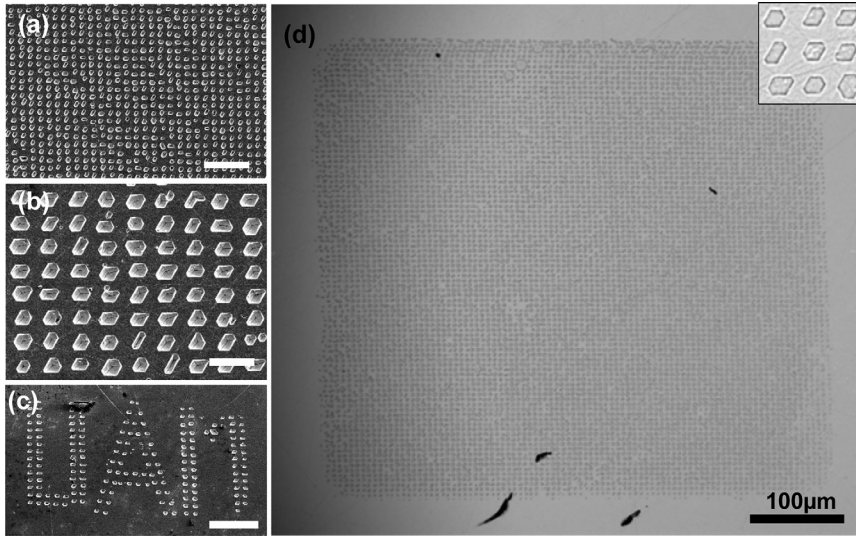


FIG. 3. Several 2D ferroelectric domain patterns in  $\text{Yb}^{3+}:\text{LiNbO}_3$ . The scale bar is (a)  $20\ \mu\text{m}$ , (b)  $10\ \mu\text{m}$ , (c)  $200\ \mu\text{m}$ , and (d)  $100\ \mu\text{m}$ .

$^2F_{5/2}(0')$  state to each of the four Stark levels of the  $^2F_{7/2}(0,1,2,3)$  fundamental state, respectively. A detailed view of the  $^2F_{5/2}(0') \rightarrow F_{7/2}(0)$  optical transition of  $\text{Yb}^{3+}$  ions is shown in Fig. 4(b). For both original and inverted regions, the emission shows identical spectral features in terms of spectral width, peak position, and lack of spectral satellites. It can be then established that the domain inversion process does not alter the local environment of  $\text{Yb}^{3+}$  centers, and therefore, the spectroscopic and laser properties of  $\text{Yb}^{3+}:\text{LiNbO}_3$  will remain unaffected. This result contrasts with those previously reported for  $\text{Nd}^{3+}$  or  $\text{Er}^{3+}$  in which the distribution of the emitting centers structure was altered by the polarization switching.<sup>12,13</sup> The different spectral behavior can be associated with the fact that  $\text{Yb}^{3+}$  ion exhibits the smallest ionic radius of the lanthanide series, so that its

incorporation produce a minor distortion in the  $\text{LiNbO}_3$  lattice and a single emitting center occupying the regular  $\text{Li}^+$  cationic site.<sup>14</sup>

The far field patterns of SHG obtained upon two different infrared ( $1.06\ \mu\text{m}$ ) pumping geometries are shown in Figs. 4(c) and 4(d). In both cases, the SHG response shows non-collinear propagation according to the 2D geometry of the domain structure, which provides several reciprocal lattice vectors (RLV),  $\mathbf{G}_{m,n}$ , within the same crystal, increasing not only the frequency conversion range but also the directions at which the quasi-phase matching (QPM) condition is satisfied. In particular, when the fundamental beam,  $\mathbf{k}_\omega$ , propagates perpendicular to the inverted domains (Fig. 4(c)), the SHG radiation is emitted in the plane perpendicular to the  $z$  axis following the expression:<sup>15</sup>

$$\frac{\lambda^{2\omega}}{n^{2\omega}} = \frac{2\pi}{|\mathbf{G}_{m,n}|} \sqrt{\left(1 - \frac{n^w}{n^{2w}}\right)^2 + 4 \frac{n^w}{n^{2w}} \sin^2 \theta}, \quad (1)$$

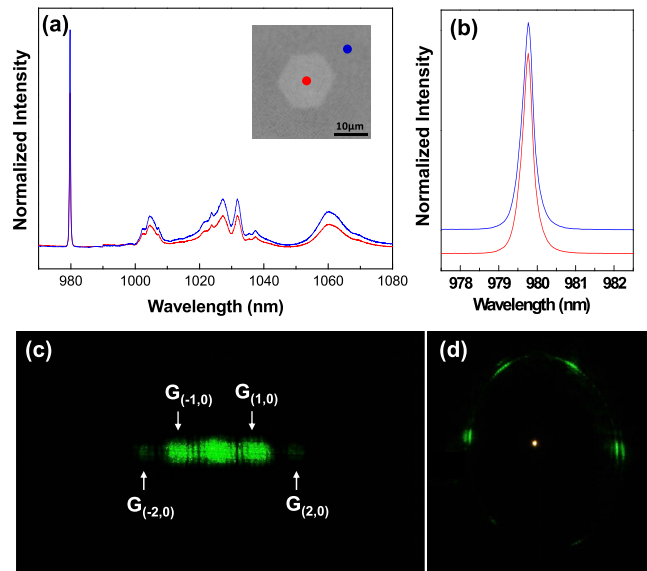


FIG. 4. (a) 10 K emission spectra collected at the virgin (non irradiated) area and domain inverted motif. The spectra have been vertically translated for the sake of comparison. (b) Detailed view of the zero-phonon transition. (c) and (d) Far field SHG patterns obtained when the fundamental beam travels perpendicular (c) and parallel (d) to the ferroelectric axis.

where  $\lambda^{2\omega}$  is the SH wavelength inside the material,  $2\theta$  is the walk-off angle between the wavevectors  $\mathbf{k}_{2\omega}$  and  $\mathbf{k}_\omega$ , and  $n^\omega$  and  $n^{2\omega}$  correspond to the refractive index of  $\text{LiNbO}_3$  crystal at the fundamental and second harmonic frequencies, respectively. Upon this configuration the recorded far field SHG pattern shows four non-collinear bright spots because of the ability of the structure to support different orders. The measured external angles were found to be  $1.38^\circ$  and  $2.80^\circ$ , which correspond to the first and second order transverse QPM processes via the  $\mathbf{G}_{0,\pm 1}$  reciprocal lattice vectors of the lattice.

In Fig. 4(d), the infrared beam is parallel to the ferroelectric domains. In this configuration, all the RLV,  $\mathbf{G}_{m,n}$  lies on the plane perpendicular to the fundamental wavevector  $\mathbf{k}_\omega$ . Therefore, according to the momentum conservation law, the SHG waves propagate with a conical angle defined by the Cerenkov angle  $\cos \theta = 2k_\omega/k_{2\omega} = n^o(\omega)/n^{o,e}(2\omega)$ . The azimuthal intensity dependence of the generated conical beams is related to that of the quadratic nonlinear effective coefficients  $d_{\text{eff}}$  of  $\text{LiNbO}_3$  which can be written in terms of the nonlinear effective coefficients  $d_{\text{eff}}^{\text{ord}}$  and  $d_{\text{eff}}^{\text{ext}}$  as

$$\begin{aligned} I_{SHG}^{ord} &\approx (d_{eff}^{ord})^2 = (d_{22}\cos(\varphi + 2\gamma))^2, \\ I_{SHG}^{ext} &\approx (d_{eff}^{ext})^2 = (d_{31}\sin\theta + d_{22}\sin(\varphi + 2\gamma)\cos\theta)^2, \end{aligned} \quad (2)$$

where  $d_{22}$  and  $d_{31}$  are the relevant nonlinear coefficients,  $\varphi$  is the azimuthal angle measured counterclockwise from the  $x$  axis, and  $\gamma$  is the polarization angle of the linearly polarized fundamental incident beam measured from the  $x$  axis ( $\gamma = 0$  for polarization along the  $x$  axis). Additionally, the Cerenkov SHG pattern shows a hexagonal distribution of more intense regions related to the nonlinear diffraction produced by the hexagonal domain walls.<sup>16</sup> The multidirectional character of the nonlinear response is then manifested. Further, the employed fundamental wavelength matches the  $1.06\ \mu\text{m}$  laser emission of  $\text{Yb}^{3+}:\text{LiNbO}_3$ , so that solid state lasers with a reliable multifunctional optical character can be envisaged.

In summary, we have reported on highly controllable ferroelectric domain inversion in  $\text{Yb}^{3+}:\text{LiNbO}_3$  laser crystal. By using DEBW, large areas of fully dense ferroelectric domains structures with diameters and separation as low as  $1\ \mu\text{m}$  have been obtained. This represents the shortest period achieved in 2D bulk optically active  $\text{LiNbO}_3$  crystal. The effect of the domain inversion process on the optical response was evaluated by linear and non-linear (SHG) optical spectroscopy and the possibility to obtain multidirectional frequency conversion processes at the  $\text{Yb}^{3+}$  fluorescence region is demonstrated. Because of the flexibility of DEBW and the significant progress achieved on engineer domain structures, this work represents a step towards the development of efficient frequency converters based on two dimensional non linear photonic laser crystals.

This work has been supported by Spanish Government under Project No. MAT2010-17443 and Comunidad de Madrid under Grant No. S2009/1756.

- <sup>1</sup>M. B. Nasr, S. Carrasco, B. E. A. Saleh, A. V. Sergienko, M. C. Teich, J. P. Torres, L. Torner, D. S. Hum, and M. M. Fejer, *Phys. Rev. Lett.* **100**, 183601 (2008).
- <sup>2</sup>L. Mateos, P. Molina, J. Galisteo, C. López, L. E. Bausá, and M. O. Ramírez, *Opt. Express* **20**, 29940 (2012).
- <sup>3</sup>T. Ellenbogen, N. Voloch-Bloch, A. Ganany-Padowicz, and A. Arie, *Nat. Photonics* **3**, 395 (2009).
- <sup>4</sup>M. O. Ramirez, P. Molina, and L. E. Bausa, *Opt. Mater.* **34**, 524 (2012).
- <sup>5</sup>E. Yraola, P. Molina, J. L. Plaza, M. O. Ramírez, and L. E. Bausá, *Adv. Mater.*, DOI: 10.1002/adma.201203176 (published online).
- <sup>6</sup>A. C. G. Nutt, V. Gopalan, and M. C. Gupta, *Appl. Phys. Lett.* **60**, 2828 (1992).
- <sup>7</sup>J. He, S. H. Tang, Y. Q. Qin, P. Dong, H. Z. Zhang, C. H. Kang, W. X. Sun, and Z. X. Shen, *J. Appl. Phys.* **93**, 9943 (2003).
- <sup>8</sup>Y. Glickman, E. Winebrand, A. Arie, and G. Rosenman, *Appl. Phys. Lett.* **88**, 011103 (2006).
- <sup>9</sup>M. Molotskii, A. Agronin, P. Urenski, M. Shvebelman, G. Rosenman, and Y. Rosenwaks, *Phys. Rev. Lett.* **90**, 107601 (2003).
- <sup>10</sup>V. Y. Shur, E. V. Nikolaeva, E. I. Shishkin, A. P. Chernykh, K. Terabe, K. Kitamura, H. Ito, and K. Nakamura, *Ferroelectrics* **269**, 195 (2002).
- <sup>11</sup>A. Lorenzo, H. Jaffrezic, B. Roux, G. Boulon, and J. GarciaSole, *Appl. Phys. Lett.* **67**, 3735 (1995).
- <sup>12</sup>V. Dierolf, C. Sandmann, S. Kim, V. Gopalan, and K. Polgar, *J. Appl. Phys.* **93**, 2295 (2003).
- <sup>13</sup>P. Molina, D. Sarkar, M. O. Ramirez, J. G. Sole, L. E. Bausa, B. J. Garcia, and J. E. M. Santiuste, *Appl. Phys. Lett.* **90**, 141901 (2007).
- <sup>14</sup>E. Montoya, A. Lorenzo, and L. E. Bausa, *J. Phys. Condens. Matter* **11**, 311 (1999).
- <sup>15</sup>V. Berger, *Phys. Rev. Lett.* **81**, 4136 (1998).
- <sup>16</sup>P. Molina, M. O. Ramirez, B. J. Garcia, and L. E. Bausa, *Appl. Phys. Lett.* **96**, 261111 (2010).